Hindawi
Journal of Nanomaterials
Volume 2024, Article ID 9504522, 15 pages
https://doi.org/10.1155/2024/9504522

Research Article

Influence of the DEA Concentration on Structural and Optical Properties of Nanodot PbS Thin Films Growth by Chemical Solution Deposition: Unveiling Dual Optical Absorption Edges

Ibrahim Alghoraibi

Department of Physics, Faculty of Sciences, Damascus University, Damascus, Syria

Correspondence should be addressed to Ibrahim Alghoraibi; ibrahim.alghoraibi@gmail.com

Received 8 September 2023; Revised 12 March 2024; Accepted 2 April 2024; Published 30 April 2024

Academic Editor: Valeri P. Tolstoy

The present paper presents a straightforward method for producing thin film layers of sulfide quantum dots (PbS-QDs) on a glass substrate using chemical solution deposition (CSD) assisted by dipcoating technique. The deposited PbS-QDs films were subjected to a comprehensive analysis using atomic force microscopy (AFM), energy dispersive X-ray (EDX) scanning electron microscopy (SEM), X-ray diffraction (XRD), UV–vis–IR absorption, and photoluminescence spectroscopic (PL) techniques to investigate the effects of varying concentrations of diethanol amine (DEA) on their morphology, crystal structure, elemental composition, light absorption, and emission characteristics. The spherical shape of the PbS-QDs was confirmed by AFM and SEM images with average sizes around 100 and 50 nm, respectively. The energy dispersive X-ray (EDX) analysis provides evidence the existence of Pb and S elements within the PbS matrix. X-ray diffraction (XRD) results validate that the deposited films exhibit high crystallinity, with a preferential orientation along the (111) plane and a face-centered cubic lattice structure of PbS. The crystallite size of PbS is measured to be 46.6 nm. Based on the optical absorption measurements, we have determined the size range of PbS nanocrystals to be between 4.3 and 11.5 nm. The optical studies reveal the presence of two optical absorption edges within the visible and infrared spectrum, two direct band gap energy, two cut-off wavelengths, two confinement energy, two Urbach energy tail, and dual emission peaks of PbS-QDs at room temperature. The analysis reveals the presence of two distinct band gap energies, one in the visible range (1.3–2.28 eV) and the other in the infrared range (0.65–0.88 eV), which can be attributed to the formation of two distinct sizes of quantum dots situated in two different layers. The first layer, deposited directly on the glass substrate, comprises quantum dots with an average size of approximately 5.2 nm, while the second layer contains quantum dots with an average size of about 9.5 nm. This ability to tune the band gap of PbS in the visible range up to the IR band (0.65–2.28 eV) is a critical feature that holds the potential for the development of innovative optoelectronic devices.

1. Introduction

Lead sulfide (PbS) belongs to the binary IVB-VIA group of semiconductors, characterized by a relatively large excitation Bohr radius ranging from 18 to 20 nm [1]. It has a direct, small bulk optical energy band gap of 0.41 eV (excitation edge of 3,200 nm at 300 K), and a high absorption coefficient of 105 cm^{-1} in visible light [2]. Owing to these properties, PbS thin films hold great potential for a wide range of technological applications, including light-emitting diodes [3], solar cells [4], IR detectors [5–7], photovoltaic [8], photodetectors [9, 10], laser, diode, electronic, optoelectronic devices [11], gas sensing [12], photocatalyst [13], and photosensing. PbS nanostructures can be synthesized in a range of shapes and sizes such as nanowires [12], nanocubes [14], flower-like nanocrystallines [15], star-like [16, 17], nanorods [18], nanoparticles [19], nanofibers [20], nanoclusters [21], and hollow PbS nanospheres [22]. These entire forms of PbS can be prepared by different deposition methods, such as spray pyrolysis [3], vacuum deposition [23], electrochemical deposition [11], chemical bath (solution) deposition (CBD or CSD) [24–26], pulsed laser deposition [27], pulsed femtosecond laser irradiation [28], sonochemical [12, 23], microwave irradiation [29], spray pyrolysis [30], flash thermal evaporation [31], hydrothermal synthesis [16, 17, 32], sol–gel technique [33], solid–vapor deposition [34], successive ionic

layer adsorption and reaction [35], green synthesis [36], microwave-assisted chemical bath deposition [37], nebulizer spray technique [38–40], spin coating [41], and radio frequency sputtering [42]. Chemical solution deposition (CSD) is a widely used and popular technique in the field of thin film technology, owing to its numerous advantages. These include its simplicity, low cost, ability to produce thin films with excellent homogeneity, low processing temperature, freedom from the need for complex vacuum equipment, and its suitability for the deposition of materials on a range of substrates. Additionally, it offers the capacity for the deposition of thin films over large areas, control over thin film properties, and the ability to manipulate the grain size of the nanocrystallites by adjusting the deposition parameters [12]: concentration of the reactants [43], reaction time deposition [15, 37, 44], temperature [19, 42, 45, 46], annealing temperature [27], pH of solution [43, 47], number of layer deposition [48, 49], complexing agent [50], coradiation [51], surfactant [52], doping such as Zn [53, 54], Cd [23, 55], Tb^{3+}ions [12], Mn [23, 48], Sm [56], Ni [23, 57] Pt [58], Cu [59], Gd [60], Ag [23, 40], Mg [61], La [62], and Cr [23, 63], effect of substrate [64], source precursor [19], and capping ligand [65]. During the chemical bath deposition (CBD) process, controlled chemical reaction kinetics are employed to regulate particle size by manipulating the availability of metal ions (M^{+2}) in the solution. It is of utmost importance to meticulously manage the ion-by-ion reaction to avoid any unintended precipitation and ensure the production of premium-quality thin films. This can be achieved by employing a stable metal ion complex, which restricts the number of free ions available in the solution. Particle size of PbS is generally affected by the reaction kinetics in the CSD process. Use of a complexing agent during CSD process alters reaction kinetics and thus particle size by controlling the availability of Pb^{2+} ions in the solution. The objective of this study was to employ the CSD method for synthesizing homogeneous PbS-QDs nanolayers on glass substrates, using three sets of films with varying concentrations of diethanol amine. The synthesized PbS-QDs thin films were characterized using multiple analytical techniques, including AFM, X-ray, EDX, SEM, UV–vis–NIR spectrophotometry, and PL. Additionally, the study presents a detailed discussion of the growth mechanism for the formation of PbS-QDs films. The best of our knowledge, there is no similar results have been reported earlier in the literature and there are not many references that discuss the possibility of controlling the absorption edge values for lead sulfide. The only reference that confirms this idea was provided by Popa et al. [66]. The study aims to prepare PbS-QDs thin films of lead sulfide with tunable absorption edges, extending from the visible to the near-infrared range, to be suitable for photovoltaic cell applications.

2. Experimental Section

2.1. Materials and Chemicals. In the experimental section, PbS-QDs thin films were deposited using a solution that contained HN $(CH_2CH_2OH)_2$, Pb $(CH_3COO)_2$, CS $(NH_2)_2$, and NaOH under various experimental conditions. The diethanol amine (DEA) used in the process was obtained from Aldrich and is a colorless, polyfunctional liquid that acts as a weak base due to being a secondary amine and a diol. DEA is soluble in water and hygroscopic due to the hydrophilic nature of its alcohol groups. Lead acetate (LA) (99.99 + %), thiourea (TU) (≥99.0%), and NaOH (Gadot grade) were also obtained from Aldrich and were used without additional purification. Deionized water was used in all experiments.

2.2. Reaction Mechanism and Deposition of PbS Films

2.2.1. Preparation of Glass Substrate. In order to fabricate PbS films, microglass plates (Ref 7101) with dimensions of 75 mm × 25 mm × 1 mm were utilized as the substrate. The quality and adhesion of the film on the substrate heavily relies on the cleanliness of the substrate surface, as it should exhibit a high level of transparency to visible light. The cleaning process began with carefully washing the glass substrates with acetone and deionized water, followed by ultrasonic cleaning using an ultrasonic bath operating at a frequency of 24 kHz and a power of 150 W at a temperature of 50−60°C for 30 min. Subsequently, the glass slides were dried with clean dry air to enhance the surface nucleation for growth of the films. After this process, the substrate was prepared for film deposition. The glass substrates coated with PbS thin films on both sides were removed and washed thoroughly with distilled water before being left to dry in an open atmosphere. The uniform surface of the glass substrate that faced the wall of the beaker during deposition was preserved for further analysis, while the other substrate surface facing the interior of the bath was treated with a nitric acid solution and removed using a cotton swab.

2.2.2. PbS Precursor Solution. $Pb(CH_3COO)_2$ and $CS(NH_2)_2$ were employed as the sources of cations (Pb^{+2}) and anions (S^{-2}), respectively, for the purpose of depositing PbS thin films onto a glass substrate. Initially, a 0.5 M solution of lead acetate was mixed with 6 ml of deionized water and magnetically stirred for 30 min until a homogeneous mixture was obtained. Following this, 1 M of sodium hydroxide (NaOH) was added to the mixture under stirring conditions for 3 min, leading to the whitening of the solution. The pH of the precursors was subsequently meticulously regulated to 12.4 ± 0.1 using a pH meter. Finally, 7 ml of a 2 M solution of $[CS(NH^2)_2]$ was added to the mixture. To avoid precipitation in the bath, control the rate reaction and to enhance the incorporation of ions on the substrate, a small quantity DEA was added as a complexing agent into the precursor solution. Three different molar concentrations (0.4, 1.2, and 2 M) of DEA were prepared separately in the same procedure as given in Table 1. The resultant solution was stirred gently for deposition of good-quality films.

2.2.3. Deposition of Nanofilm. The pretreated microscope glass plates were vertically dipped by using a homemade dipcoating apparatus into a reaction nanosol to have thin film deposition for 30 min at room temperature. Upon completion of the deposition process, the samples were extracted from the solution at a constant speed of 200 μm/s and

Table 1: The measured values of mean diameter (d), mean height (h), average line surface roughness (Ra), line root-mean-square roughness (L_{rms} = Rq), average area surface roughness (Ra), area root-mean-square roughness (S_{rms} = Sq), thickness, and growth rate of the PbS-QDs thin films deposited at various molarities of DEA.

Sample no.	DEA (M)	D (nm)	h (nm)	Ra (nm)	Rq (nm)	Sa (nm)	Sq (nm)	Thickness (nm)	Growth rate (nm/s)
S1	0.4	89.4	6.8	5.5	6.9	5.7	7.0	78.6	0.06
S2	1.2	94.6	13.6	5.8	7.2	6.3	7.6	84.6	0.05
S3	2.0	117.5	18.2	7.5	9.2	7.5	9.3	126.8	0.12

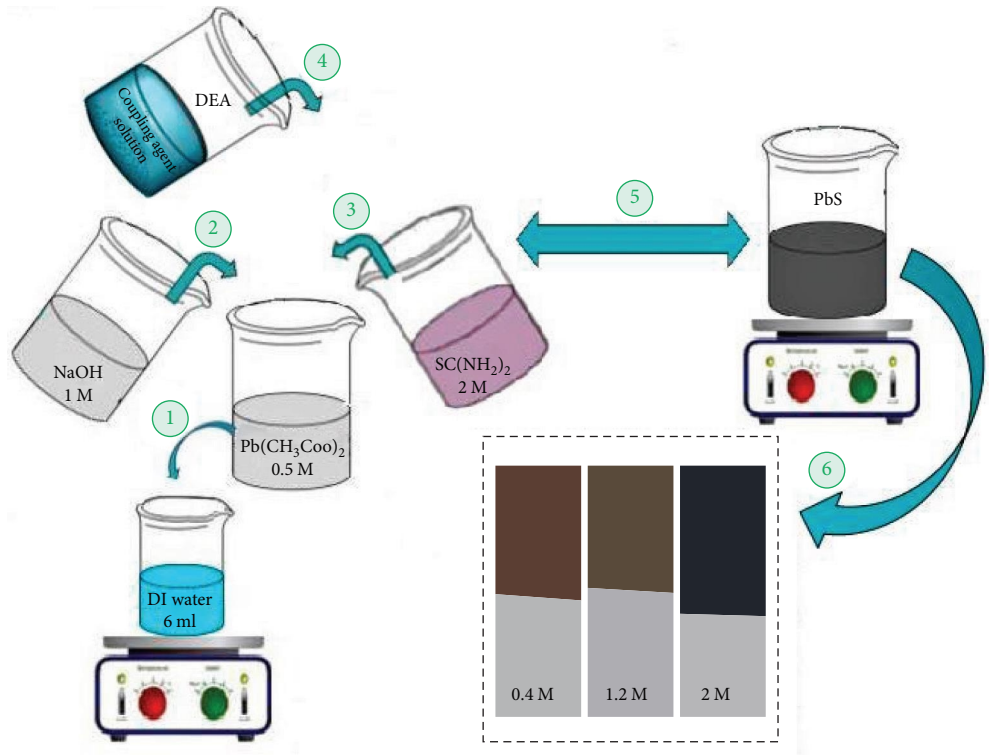

Figure 1: Schematic diagram of preparation of PbS films on glass substrates.

subsequently underwent ultrasonic rinsing in acetone and distilled water for 2 and 10 min, respectively, in order to eliminate the nonadherent PbS layer. Finally, the samples were air-dried at room temperature. The photographs of PbS thin films are shown in Figure 1. The photograph clearly shows the uniform, grayish-colored PbS thin films, and well adhered to the glass substrate. During the dipping process, thin films are stuck onto the two faces of the substrate. Note that the layers deposited on the side of the substrate that faced the wall of the beaker were used for all measurements. The thickness of deposited film was estimated from the mass change of the glass substrate before and after coating procedure using a high precision weight balance with 0.00001 gr standard deviation and from the known bulk density of PbS (7.569 gr/cm^3).

2.3. Mechanism of Thin Film Formation. The chemical reaction mechanism for the formation of lead sulfide is influenced by the experimental conditions. The formation of PbS occurs when the ionic product of Pb^{2+} and S^{2-} ions surpasses the solubility product. The rate of growth for PbS thin films is predominantly influenced by the rate of release of Pb^{2+} ions from the complex and the decomposition of thiourea in an alkaline aqueous medium. The process of (PbS) thin film formation and its growth can be described via the mechanism of the following reaction: In alkaline solution, the hydrolysis of lead acetate leads to the formation of $Pb(OH)_2$:

$$Pb(CH_3COO)_2 + 2NaOH \longrightarrow Pb(OH)_2 + 2CH_3COON, \quad (1)$$

$$Pb(OH)_2 \longrightarrow Pb^{2+} + 2OH^-. \quad (2)$$

Thiourea decomposes in alkaline solution and produces HS^- ions:

$$SC(NH_2)_2 + OH^- \longrightarrow CH_2N_2 + H_2O + SH^-, \quad (3)$$

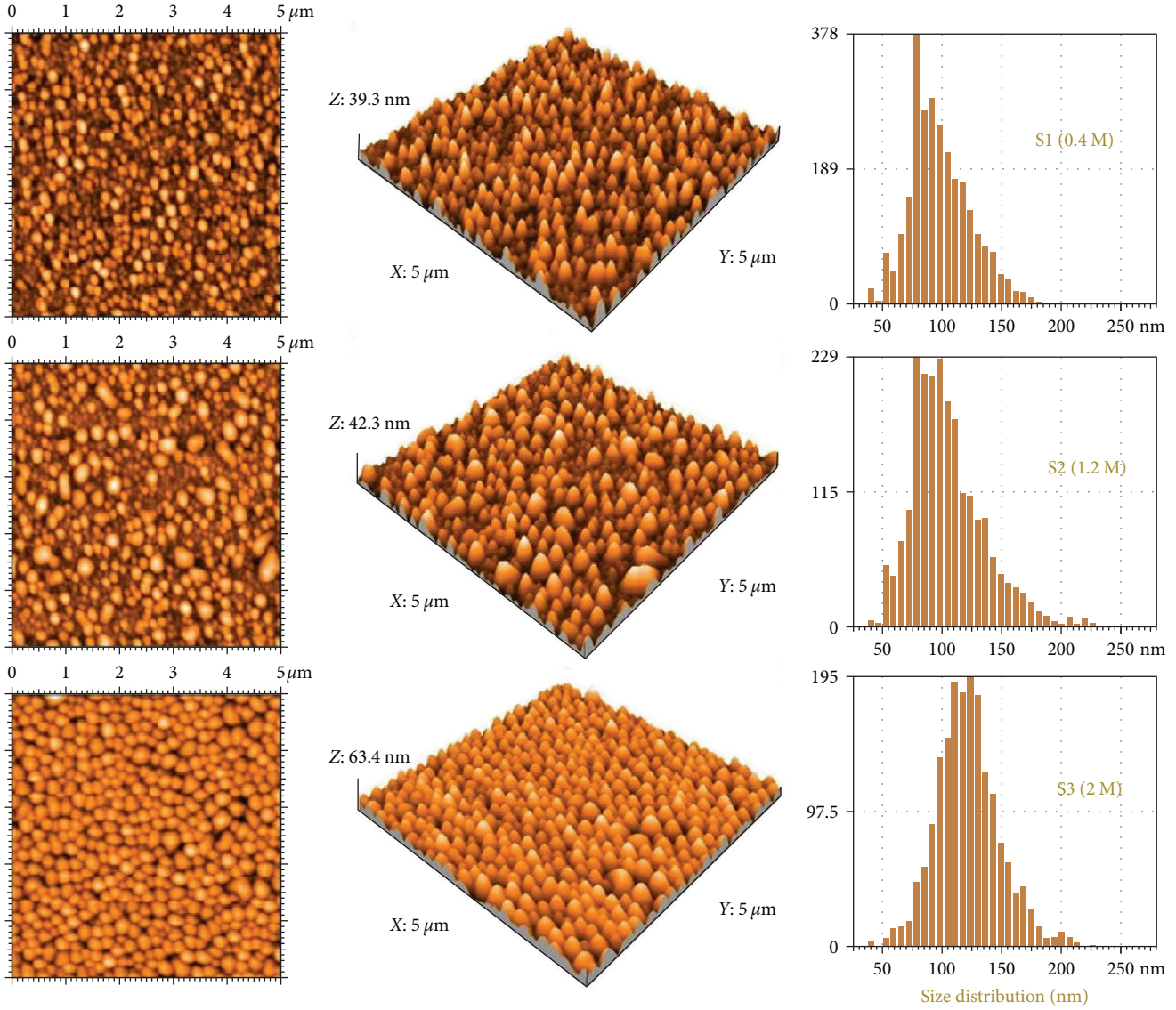

Figure 2: Atomic force microscopy (AFM) images of the 2D and 3D structures ($5 \times 5\,\mu m^2$) and the size distribution of PbS-QDs thin films grown on glass substrates at varying concentrations of DEA, including 0.4 M (S1), 1.2 M (S2), and 2.0 M (S3).

$$SH^- + OH^- \longrightarrow S^{2-} + H_2O, \quad (4)$$

$$Pb^{2+} + S^{2-} \longrightarrow PbS\downarrow. \quad (5)$$

The solution color was changed to brown and then dark gray after about 2 min, which indicates the PbS formation. Pb^{2+} ion complexes with DEA initially, forming [Pb^{2+} DEA^-]. The complex later decomposes, releasing Pb^{2+} ions that bond with S^{2-} ions to form PbS. The addition of a complexing agent to a Pb salt solution influences the release rate of Pb^{2+} ions. The complexing agent forms lead complex species that, upon dissociation, release variable concentrations of Pb^{2+} ions. These ions, along with liberated sulfide ions, migrate to the substrate surface, where they react to form a PbS thin film. This process modifies the rate of Pb^{2+} ion release, facilitating controlled film formation. The mechanism of this film formation can be elucidated by the ensuing chemical reaction:

$$Pb^{2+} + DEA \longrightarrow Pb^{2+}DEA^-_{(complex)}, \quad (6)$$

$$Pb^{2+}DEA^-_{(complex)} + S^{2-} \longrightarrow PbS + DEA. \quad (7)$$

3. Results and Discussion

This research paper aimed to optimize the chemical process of depositing semiconducting thin films of PbS-QDs on glass plates for optical applications. The study focused on investigating the impact of varying concentrations of complexing agents on the morphology and optical properties of the PbS-QDs films. Structural characterization, morphological analysis, and elemental composition were performed using AFM, SEM, EDX, XRD, and DLS. Optical properties were evaluated through absorption and transmission measurements, as well as analysis of parameters such as absorption coefficient,

extinction coefficient, confinement energy band gap, Urbach energy, and PL.

3.1. Atomic Force Microscopy Analysis. The surface topology, quantum dot size, surface roughness, and film thickness of the PbS were evaluated as a function of concentrations of DEA using atomic force microscopy (AFM, Nanosurf easyScan2, Switzerland) to optimize the chemical process for growing PbS-QDs semiconducting thin films on glass plates. AFM measurements were conducted in tapping mode (Tap190 Al-G, NanoSensors™, Neuchatel, Switzerland) under ambient air conditions. The tip deviation sensitivity and scanner resolution were 0.2 nm, and the scan resolution was set to 256×256 points for all observations. AFM images and particle size distributions of the PbS-QDs thin films deposited using different concentrations of DEA (0.4 M, S1; 1.2 M, S2; 2.0 M, S3) are illustrated in Figure 2. The other parameters were kept constant (time deposition 30 min, 0.5 M lead acetate, 2M thiourea, 1 M sodium hydroxide, a pH of 12.4 ± 0.1 for sodium hydroxide and a temperature of 25°C).

These images demonstrate the effect of varying the molar concentration of the complexing agent on the size and quality of the PbS-QDs films. It is evident that the films are of high quality and possess uniform morphology, covering the entire substrate surface. The PbS-QDs adopt a uniformly spherical shape and exhibit a range of dimensions that are dependent on the concentration of the complexing agent. The films prepared using 0.4 M of DEA (Figure 2(S1)) exhibit a uniform distribution of isotropic dot sizes with high density ($1{,}4.10^{10}$ particle/cm^2) and an average diameter ($d = 89.4 \pm 5$ nm) and height ($h = 6.8 \pm 1$ nm). Meanwhile, the PbS-QDs grown with intermediate concentration of DEA (1.2 M) (Figure 2(S2)) have an average diameter of 94.6 nm, a mean height of 13.6 nm, and owing to coalesce of smaller dots into larger dots or agglomeration of the dots by the Ostwald ripening process. At higher concentrations of DEA (2.0 M), larger dots tend to coalesce together to form interconnected nanodots without formation of clusters (Figure 2(S3)). When increasing the concentration of DEA, the PbS-QDs mean diameter and height are increased to 117.5 and 18.2 nm, respectively.

Table 1 presents the line (profile) roughness parameters (Ra, Rq), area (surface) roughness parameters (Sa, Sq = RMS), thickness, and growth rate of the PbS thin films grown with varying DEA concentrations. The results show that increasing the molarities of DEA results in an increase in the mean height (h) and roughness (Ra, Rq, Sa, and Sq) of the films due to the formation of larger domed dots and a more complete layer with a decreased fraction of voids. It is noteworthy that the reported values are mean values, subject to statistical fluctuations that are contingent on the position of the measurement on the samples. To minimize these errors, multiple readings of each parameter were performed in various locations on the sample surface. The experimental parameters and AFM data are summarized in Table 1.

As we can see from AFM images, any increase in DEA concentration causes a speed-up formation of PbS dots in the development of average dot sizes and also their agglomeration.

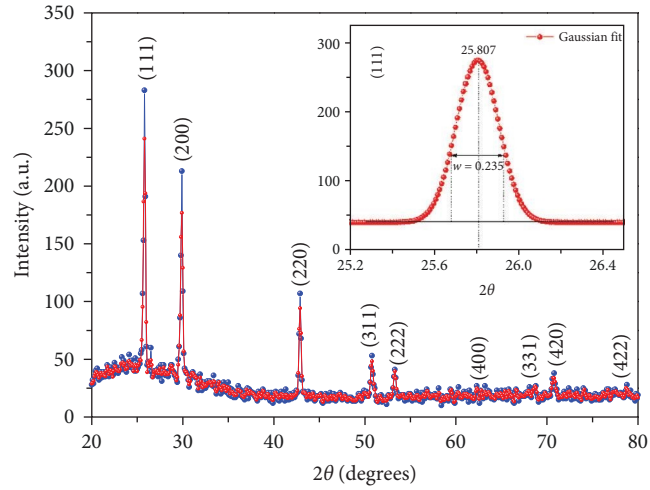

FIGURE 3: Diffractograms of as-deposited PbS-QDs thin film with DEA concentration = 0.4 M. The inset shows the Gaussian fit for (111) Bragg peak.

This is probably due to the rate of ion–ion exchange being strongly influenced by the amount of DEA, which in turn affects the growth rate of the film. Therefore, at a higher deposition concentration, the deposition rate, and film thickness increase to 0.12 nm/s and 126.8 nm, respectively (Table 1), while the rate of precipitation forming is slow; consequently, the PbS dots have enough time to grow. The presence of DEA with different concentrations during the formation of the PbS probably causes a change in the mechanism and kinetics of the reaction. The thickness of deposited film was estimated from the mass change of the glass substrate before and after the coating procedure using a high precision weight balance with 0.00001 gr standard deviation and from the known bulk density of PbS (7.569 gr/cm^3). Thin film growth is controlled by the ion-by-ion deposition kinetics of chalcogenide on nucleating sites that exist on the immersed surfaces. At the outset, the film's growth rate is low because it takes a certain period of incubation to produce crucial nuclei on a clean surface from a homogeneous system. Once nucleation occurs, the film's growth rate rapidly increases until the rate of deposition equals the rate of dissolution. The film eventually achieves its maximum thickness, which is referred to as the terminal thickness. An increase in the concentration of complexing ($DEA^-_{(complex)}$) ions leads to a reduction in the concentration of the metal ion (Pb^{2+}) and consequent decline in the reaction rate and precipitation. This results in the formation of larger quantum dots and a correspondingly increased terminal thickness of the film. Additionally, the quantum dots tend to exhibit uniform coverage of the substrate.

3.2. Chemical Composition and Scanning Electron Microscopy Analysis. The as-deposited PbS-QDs thin films were subjected to analysis of their elemental composition and morphology using SEM and EDX techniques. The EDX spectra presented in Figure 3 confirm the presence of two elements, Pb and S, in all the thin films deposited on glass substrate at different concentrations of DEA. The Pb/S atomic percentages ratio was found to be 1.2. The EDX analysis results for the as-deposited films, including the weight

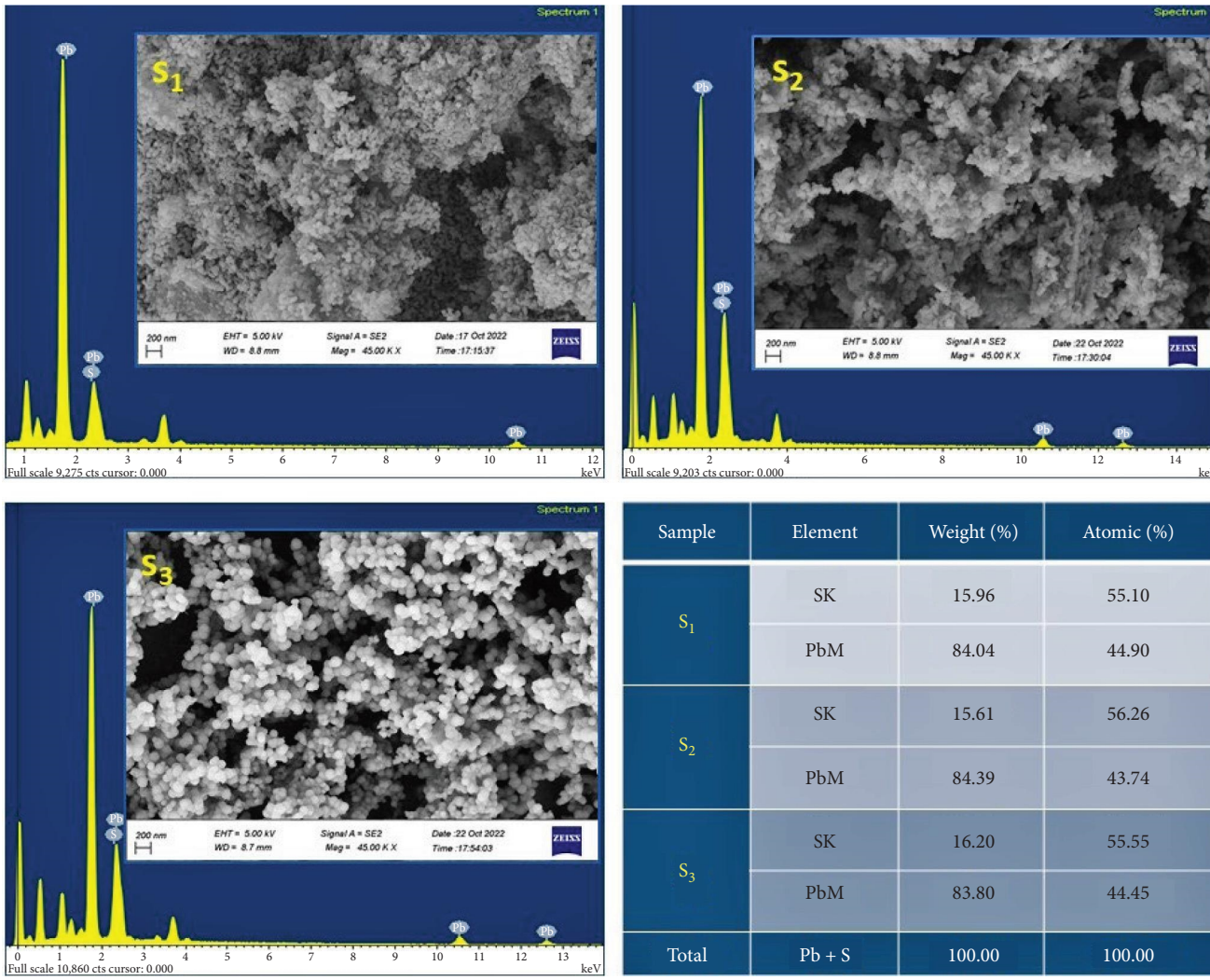

Sample	Element	Weight (%)	Atomic (%)
S_1	SK	15.96	55.10
	PbM	84.04	44.90
S_2	SK	15.61	56.26
	PbM	84.39	43.74
S_3	SK	16.20	55.55
	PbM	83.80	44.45
Total	Pb + S	100.00	100.00

FIGURE 4: SEM images and EDX spectra of the films deposited with DEA concentrations of 0.4 M (S1), 1.2 M (S2), and 2 M (S3).

and atomic percentage concentrations, are presented in the table included in the insets of Figure 4.

The analysis confirms that the PbS thin films exhibit high purity and do not include typical impurities, consistent with the XRD findings. Any extra peaks noticed in the EDX spectra are attributed to X-ray emission from the glass substrate. The morphology and size of the PbS-QDs thin films deposited at different DEA concentrations (0.4, 1.2, and 2.0 M) were examined by SEM imaging, as shown in Figure 4(S1–S3). The SEM images reveal a smooth and uniform surface morphology of the thin films that completely cover the substrate, indicating their high quality. The dots formed were spherical in shape, and their average size was found to be 34.1, 41.8, and 72.2 nm at low, medium, and high concentrations of DEA, respectively. The size of the dots increased with an increase in DEA concentration, and they tend to agglomerate.

3.3. X-Ray Crystallography Analysis. A single concentration (0.4 M) of DEA was analyzed by X-ray diffraction (XRD). The XRD spectra of the deposited PbS thin films are presented in Figure 3, recorded in the range of 20°–80°. The spectrum shows nine characteristic peaks at 2θ values of approximately 26°, 30°, 43°, 51°, 53°, 62°, 68°, 71°, and 78°, corresponding to the indexing Bragg's reflections planes (111), (200), (220), (311), (222), (400), (331), (420), and (422) orientations. These peaks are consistent with standard JCPDS data card no. 05-0592, confirming the cubic structure of PbS. The sharpness of XRD peaks suggests that the thin films were well crystallized. To determine the crystallite size and broadening (W) for the highest peak (111), modeling was performed for the corresponding preferred peak (111) using Gauss and Lorentz functions (shown in the inset of Figure 3).

The (111) peak is the highest and preferred orientation of all the films, and the average nanocrystallite size of PbS was evaluated using the *Scherrer* formula from (111) XRD peak ($D_{(111)} = 0.94\lambda/\beta \cos\theta_{(111)}$) (Equation (1)) [67]. The microstrain ($\varepsilon = \beta \cos\theta_{(111)}/4$) (Equation (2)) [68] and dislocation density ($\delta = 1/D^2{}_{(111)}$) (Equation (3)) [69] were calculated to quantify the defects of the PbS film. The preferential crystallite orientation was determined by calculating $TC_{(111)} = (I_{(111)}/(I_{0(111)}))/(\sum N^{-1} I_{(111)}/(I_{0(111)})) \times 100\%$ (Equation (4)) [70]. The values of β, D, ε, δ, and TC were tabulated in Table 2.

Table 2: Structural XRD parameters peak broadening (β), crystallite size (D), dislocation density (δ), microstrain (ε), and texture coefficient calculated from the (111) peak ($TC_{(111)}$) of PbS-QDs.

Sample nano-PbS	2θ (degree)	β (rad)	D (nm)	δ (nm^{-2})	ε ($Lin^{-2}{\cdot}m^{-4}$)	$TC_{(111)}$ (%)
DEA (0.4 M)	25.81	0.0041	46.6	4.6×10^{-4}	5.73×10^{-2}	6.02

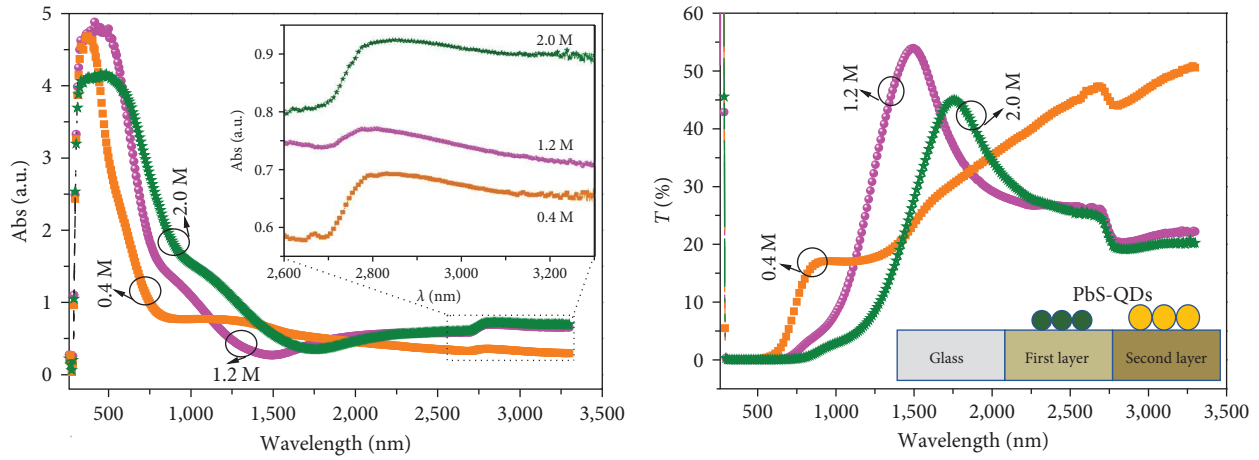

Figure 5: Optical absorbance (a) and transmittance (b) versus wavelength of the PbS-QDs thin films deposited at different concentrations of DEA as complexing agent onto glass substrate. Insets of (a): magnification of the absorption range of 2,600–3300. Insets of (b): the photographs of the PbS layers.

The XRD spectra show that the PbS thin films deposited using 0.4 M of DEA had well-crystallized cubic structure with an average nanocrystallite size of 46.6 nm. The abundance of crystals oriented in the (111) direction was higher, as indicated by the higher value of TC (111).

3.4. Optical Studies. The optical characteristics of the thin films were assessed via Varian Cary 5,000 UV–vis–NIR spectrophotometry under normal incidence of light in the wavelength range of 260–3,300 nm. The absorption and transmittance spectra of the as-deposited samples with various concentrations of DEA, 0.4, 1.2, and 2 M, are shown in Figure 5. The spectra exhibit broad and pronounced absorption edges at approximately 750, 900, and 1,130 nm for the films grown with DEA concentrations of 0.4, 1.2, and 2.0 M, respectively. This behavior is attributed to the change in the films' thickness and the size of PbS-QDs, which leads to a shift toward longer wavelengths due to the quantum size effect [71]. In addition to the absorption maximum, absorption bands were observed in the infrared range of 2,600–3,300 nm for all spectra. The insets of Figure 5(a) illustrate other absorption thresholds, corresponding to electron excitation from the valence band to the conduction band. The transmittance spectra in Figure 5(b) show a change with the increase in DEA molarity. The low transmittance was observed in UV–vis region and this is attributed to high absorption of dots at these wavelengths, while high transmittance was observed in the near-infrared region. There are three peaks at 882, 1,500, and 1,760 nm for 0.4, 1.2, and 2.0 M, respectively.

In Figure 6, the optical absorption coefficient of the PbS thin films is presented as a function of photon energy in the range of 280–3,100 nm. The results show that the absorption coefficient values for all samples are within the range of 10^5–10^6 cm^{-1}, indicating the presence of a direct optical band gap energy in the prepared PbS-QD thin films. These findings satisfy the criterion for using Tauc-plot analysis, which is suitable for absorption coefficient values greater than 10^4 cm^{-1}.

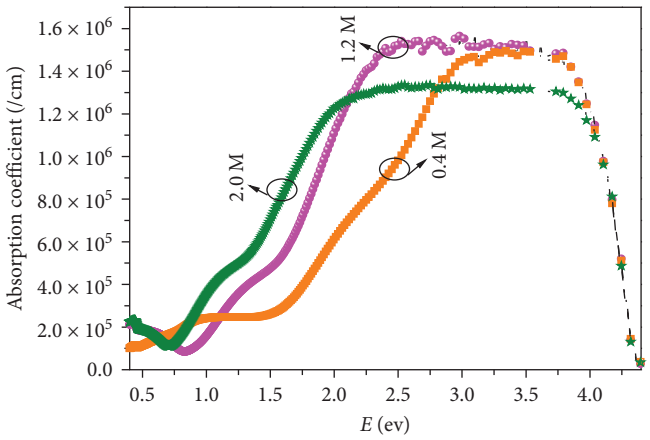

Figure 6: Optical absorption coefficient a function of photon energy of the PbS-QDs thin films deposited at different concentrations of DEA.

The extinction coefficient can be calculated using the relation: $k = \alpha\lambda/4\pi$. Figure 7 illustrates the dependency of the extinction coefficient on wavelength. It shows a sharp increase in the visible region which can be attributed to the

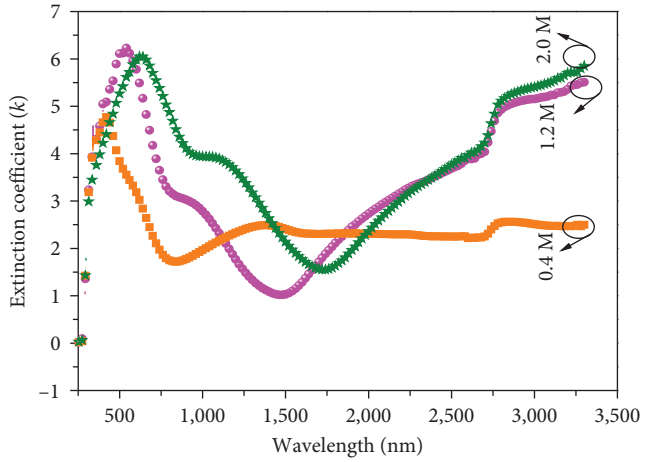

FIGURE 7: Extinction coefficient graphs vs. wavelength of the PbS-QDs thin films deposited at different concentrations of DEA.

strong absorption of incident photons in the near of the band gap.

In order to determine the direct optical band gap of PbS-QD semiconducting thin films synthesized at various concentrations of DEA, the *Tauc's* relationship was used to calculate the values of the band gap using an equation $(ahv = A(hv - E_g)^n)$ (Equation (5)) [72], where a is absorption coefficient $(a = -10^7 \frac{\ln(T)}{t})$ (Equation (6)), A is a constant related to the details of conduction and valence bands, h is Planck's constant, v is photon frequency, E_g is optical band gap and parameter n depends on the transmission type and is equal to 1/2 for allowed direct transmission.

Using the last data, the direct band gap energy of PbS thin films was estimated by plotting a graph between $(\alpha hv)^2$ versus hv, as shown in Figure 8. The optical band gap of the films can be evaluated by extrapolating the straight-line portion to the hv axis at $\alpha = 0$. In fact, the close examination of the precedent curve shows that there are two absorption thresholds for each sample, the first one is in the visible and near-infrared (at about 0.544–0.954 μm) and the other is in the near-infrared and short-infrared (at about 1.409–1.908 μm). This can be clearly seen with the linear adjustment for each region in Figure 8. The optical band gap of the PbS film coated at 0.4 M concentration is the highest (2.28 eV) and it decreases with increases in DEA concentration and attains a minimum value of (1.30 eV) for the film coated at 2.0 M concentration. An increase in the crystallite size of the film coated at 2.0 M concentration (as shown in Table 1) is the reason for the decreased band gap obtained at that concentration. The bigger particle size, the lower quantum size confinement and thus the smaller the band gap, leading to higher wavelength for the absorption edge (Figure 8). The calculated band gap values for each sample (E_{g1} and E_{g2}) are listed in Table 3, the two different absorption thresholds are correlated with the size of nanocrystallites in the thin film, the first one is in the visible region (2.28–1.30 eV, $\lambda_{\text{cut-off}} \cong 700$ nm) corresponds to nanocrystallites of small size (4.3–6.1 nm) and the second one is in the short-infrared (0.88–0.65 eV, $\lambda_{\text{cut-off}} \cong 1{,}600$ nm) is due

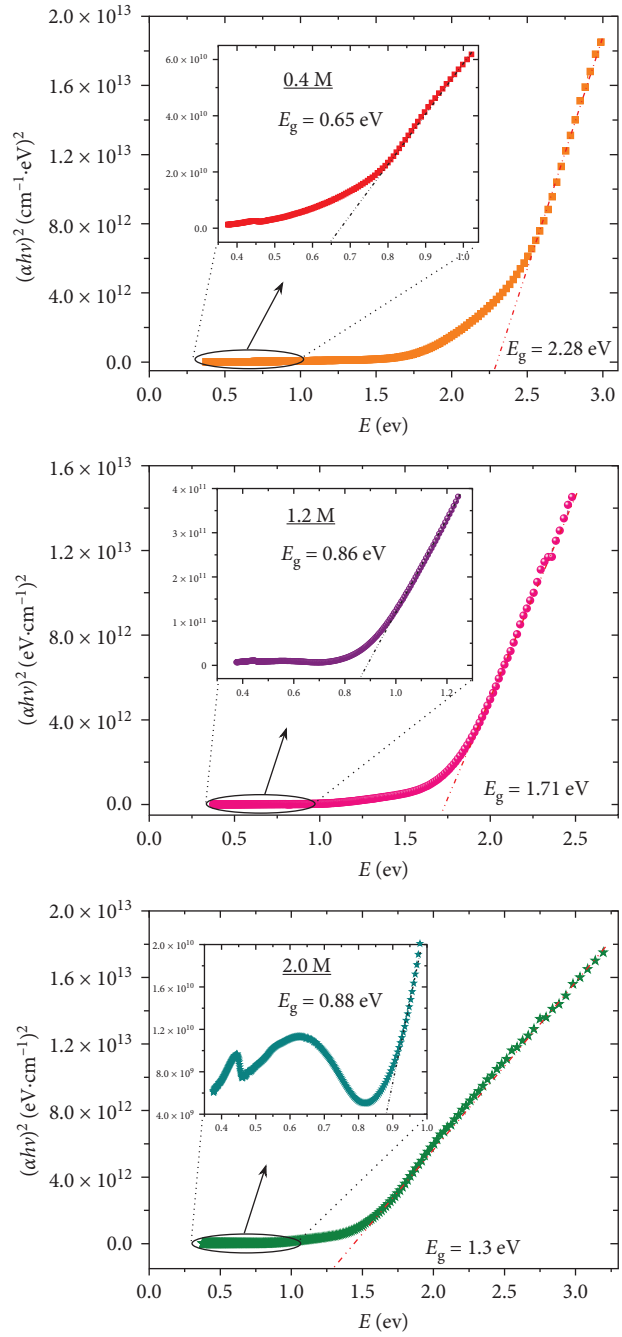

FIGURE 8: Plots of $(\alpha hv)^2$ vs. photon energy for PbS-QDs thin films deposited at different concentrations of DEA. The insets show the magnified view of the fitted lines.

to nanocrystallites of larger size (11.5–8.4 nm). This confirms that, for all these cases, the band gap increases with decreasing nanocrystallites size. Obtained band gap values for PbS thin films deposited are higher than those reported in the literature [71].

The Brus's [73] model, utilizing the effective mass approximation (EMA), can be employed to determine the crystallite size based on the relationship between the band gap of the nanostructure and the crystallite radius. Using the

Table 3: Summary of band gap values, cutoff wavelength, crystallite size, confinement energy, and Urbach energy tail values of PbS-QD films, as a function of complex agent molarity of DEA.

Sample no.	E_{g1} (eV)	$\lambda_{cut\text{-}off1}$ (nm)	$D1$ (nm)	E_{1confi} (eV)	E_{U1} (eV)	E_{g2} (eV)	$\lambda_{cut\text{-}off2}$ (nm)	$D2$ (nm)	E_{2confi} (eV)	E_{U2} (eV)
S1: 0.4 M	2.28	544	4.3	1.93	0.554	0.65	1,908	11.5	0.266	0.508
S2: 1.2 M	1.71	725	5.1	1.358	0.596	0.86	1,442	8.5	0.485	0.241
S3: 2.0 M	1.30	954	6.1	0.938	0.721	0.88	1,409	8.4	0.505	0.258

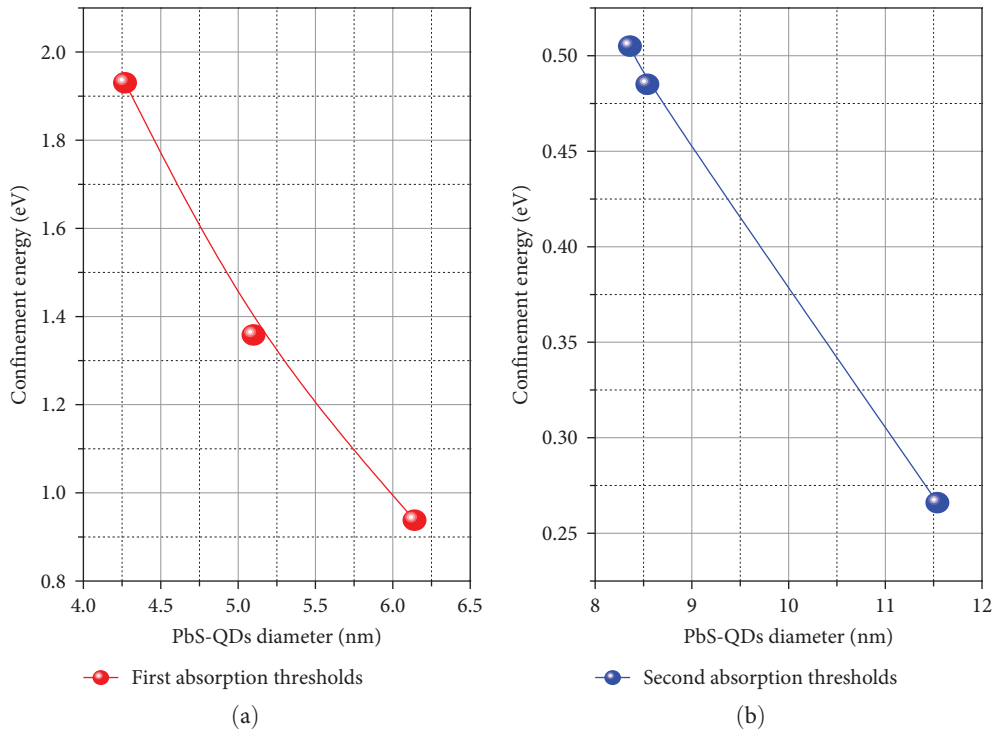

Figure 9: Variation of ground state confinement energy with diameter of PbS-QDs thin films deposited at different concentrations of DEA: (a) first and (b) second absorption thresholds.

first approximation parabolic bands model, the EMA substitutes the mass of the electron and hole with effective masses (m_e^* and m_h^*) and considers an exciton confined to a spherical volume of the crystallite. By applying the *Brus* equation, the energy of quantum confinement ($\Delta E = E_{g(QD)} - E_{bulk}$) is directly correlated to the nanocrystal radius (R):

$$E_{g(nano)} = E_{bulk} + \frac{h^2}{8R^2}\left[\frac{1}{m_e^*} + \frac{1}{m_h^*}\right] - \frac{1.786e^2}{4\pi\varepsilon_0\varepsilon_r R}. \quad (8)$$

The *Brus* equation was employed to investigate the confinement effect in PbS-QDs, where R represents the radius of the crystallite, and $E_{g(nano)}$ is the excitonic absorption peak of the nanoparticle. Additionally, $m_e{}^*$ ($m_e{}^*{}_{PbS} = 0.085\ m_o$) and $m_h{}^*$ ($m_h{}^*{}_{PbS} = 0.085\ m_o$) denote the effective masses of the electron and hole, respectively, while e represents the electric charge, and $\varepsilon = 17.3$ is the dielectric constant of PbS, and ε_o is the vacuum permittivity constant. The *Brus* equation yielded calculated diameters for PbS nanocrystallite at the first absorption thresholds of 5.1, 4.3, and 6.1 nm (≅*Bohr* radius 18 nm) and at the second absorption thresholds of 11.5, 8.5, and 8.4 nm for different concentrations of DEA (0.4, 1.2, and 2 M, respectively). Investigation revealed two different sizes of quantum dots in two different layers, with the first layer having an average nanocrystal size of about 5.2 nm and the second layer having an average nanocrystal size of about 9.5 nm (as shown in the inset of photographs in Figure 5(b)). The crystallite size PbS-QDs was shown to be smaller than the exciton Bohr radius in PbS (18 nm), thus indicating the strong quantum confinement effect. The graphs in Figure 9 of ground state confinement energy versus the size of PbS-QDs for the first and second absorption thresholds illustrate that the ground state confinement energy is inversely proportional to the size. Consequently, as the diameter increases, the confinement energy decreases but never reaches zero, meaning that the lowest possible energy for the quantum dot sample is not zero. Furthermore, confinement commences when the diameter of PbS-QDs is comparable or of the order of the exciton *Bohr* radius. As a result, the crystallite size determined by the *Brus* model differs from those determined using XRD.

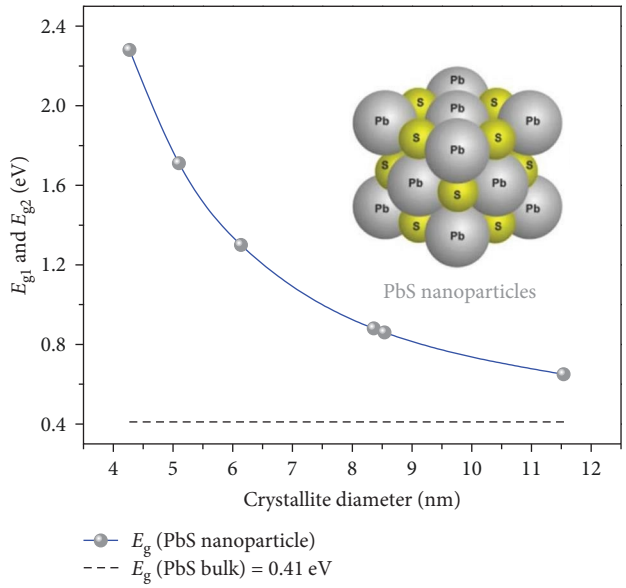

FIGURE 10: E_{g1} and E_{g2} plotted as function of crystallite diameter of PbS-QDs thin films deposited at different concentrations of DEA. Dotted line denotes the bulk PbS band gap.

The relationship between the energy gaps (E_{g1} and E_{g2}) and the diameters of deposited PbS-QDs is shown in Figure 10, which was obtained from the data presented in Figure 8. The results indicate that the energy gap increases as the crystallite size decreases. This observation can be attributed to the quantum size effects [74], which arise due to the confinement of energy levels within small potential wells. As the crystal size becomes smaller, the distance between energy levels increases. The energy gaps in the nanocrystalline films are found to be relatively high compared to that of bulk crystalline PbS (0.41 eV). Notably, a significant change in the energy gap is observed in the first stage of growth.

Urbach's empirical formula may be used to describe the exponential dependence of the absorption coefficient$\alpha < 10^4$ cm^{-1} [75]: $a(v) = a_0 \exp\left(\frac{hv}{E_U}\right)$ (Equation (8)) [76], where a_0 is a constant and E_U (Urbach energy) is an energy which is often interpreted as the width of the tail of the localized states associated with the amorphous states in the forbidden band. The relationship between the logarithm of the absorption coefficient ($\ln(\alpha)$) and photon energy for the films deposited at different DEA concentrations (0.4, 1.2, and 2 M) is shown in Figure 11, with E_{U1} and E_{U2} for the two absorption edges calculated from the reciprocal of the straight-line slopes and presented in Table 3. Table 3 illustrates an inverse relationship between the band gap energy (E_{g1} and E_{g2}), confinement energy ($E1_{confi}$ and $E2_{confi}$), and Urbach energy of PbS thin films. A minimum value of E_U suggests a very weak absorption tail due to minimized defects and impurities, improving the optical properties of the prepared films. The variation in the optical band gap with the complexing agent concentration may be attributed to the change in quantum dot size and structural disorder in the films, as observed from Urbach energy analysis.

3.5. Photoluminescence Studies. Figure 12 displays the photoluminescence emission spectra of the nanocrystalline PbS thin film at room temperature. The emission spectrum

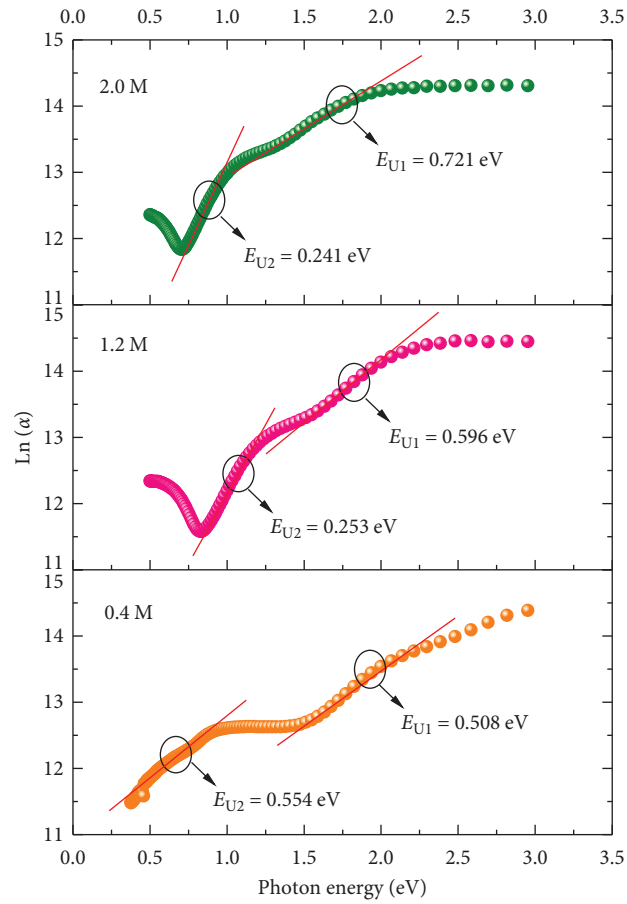

FIGURE 11: Logarithm of absorption coefficient as function of the photon energy for as-deposited PbS-QDs thin film at different concentrations of DEA.

exhibits two peaks, one at 540, 542, and 545 nm, which corresponds to the recombination of the electron and hole pair [38], and another as a shoulder at 659, 662, and 691 nm for concentrations of 0.4, 1.2, and 2.0 M, respectively. The shoulder peak is attributed to the various nanocrystallite sizes of PbS. It is noteworthy that these observed peaks are in good agreement with the absorption edges observed in the absorption spectra. The remaining two peaks observed at longer wavelengths, 546 nm and approximately 672 nm, are due to transitions in the nanocrystalline PbS-QDs films [25].

3.6. Characterization PbS Powder. After terminating the reaction and completing the deposition of the films by CSD process, the collected PbS nanopowder was subjected to multiple washes with DI water and ethanol in a sequential manner, followed by drying at 50°C. The morphological and quantitative analysis of as-prepared PbS nanopowder is examined by dynamic light scattering (DLS), zeta value, SEM, and EDX. Particle average size distribution of the resulting powder was analyzed by using DLS. Figure 13 shows the PbS-NPs are mainly uniform and monodisperse with the average range of particle size distribution is 56 nm. The zeta potential of the PbS nanopowder dispersed in water was measured, revealing a sharp peak at −9 mV, as depicted

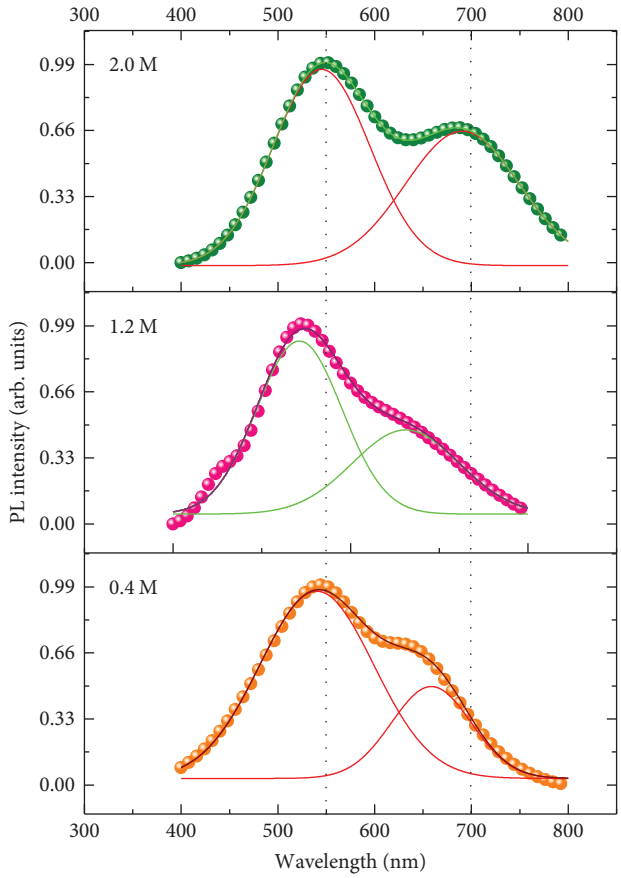

FIGURE 12: PL intensity spectrum fitted with multiple Gaussian profiles of PbS-QDs/glass thin films as-deposited at different concentrations of DEA, excited at 458 nm from the Ar^+ laser.

in Figure 13. This negative value suggests that the surface of PbS-NPs is negatively charged, resulting in weak repulsive forces between particles and leading to particle aggregation in the medium. The spherical and uniform morphology of all quantum dots, with an average size of approximately 34 nm, was confirmed by SEM images. Notably, the nanoparticle size measured by DLS was larger than that observed by SEM, reflecting the fact that DLS measures the hydrodynamic diameter of the particles while SEM determines the diameter of dry particles. Additionally, EDX analysis was conducted to determine the elemental composition of the resulting powder, and the results are presented in Figure 13.

In EDX profile, numerous well-defined peaks were evident related to Pb and S, which clearly support the fact that the as-prepared powder is the content of Pb and S. Other than this, while weaker signals from Na and O atoms were detected as well, which may originate from alkaline medium and organic compounds (DEA) or to the exposure of the powder to air, and adsorption of H_2O and CO_2. The inset table displayed the weight and atomic concentrations of Pb, S, Na, and O.

4. Conclusion

We have successfully deposited mirror-like, nanostructured PbS quantum dot films with tunable band-gap energies directly onto glass plates using different molar concentrations of diethanolamine (DEA) as a complexing agent via the CSD dipcoating method. The presence of the complexing agent in the bath has been observed to affect the rate of deposition and the crystallite size of the deposited lead sulfide film. The EDX analysis validates the high quality of the thin films, without any commonly encountered impurities. These findings align with the observations from the XRD analysis. Characterization of the as-deposited thin films has revealed their well-crystalline nature and good optical properties. Our photoluminescence study has indicated the occurrence of dual emission peaks in the visible region, specifically around 546 and 672 nm. The optical measurements indicate that the prepared films are composed of two distinct layers with varying particle dimensions. Also, we have determined that two distinct absorption edges. The first edge, ranging from 0.65 to 0.88 eV, is linked to PbS nanocrystals with sizes ranging from 8.4 to 11.5 nm in the initial layer (glass/PbS). The second absorption edge, observed at 1.3–2.28 eV, indicates the formation of nanocrystals below 6.1 nm in the upper second layer (PbS/PbS). This flexibility in varying the band gap of PbS-QDs in the range of 0.49–2.28 eV makes them a better candidate for solar energy conversion in the near-infrared region and opens the door for the creation of a new types of optoelectronic elements. This study presents a straightforward method for the

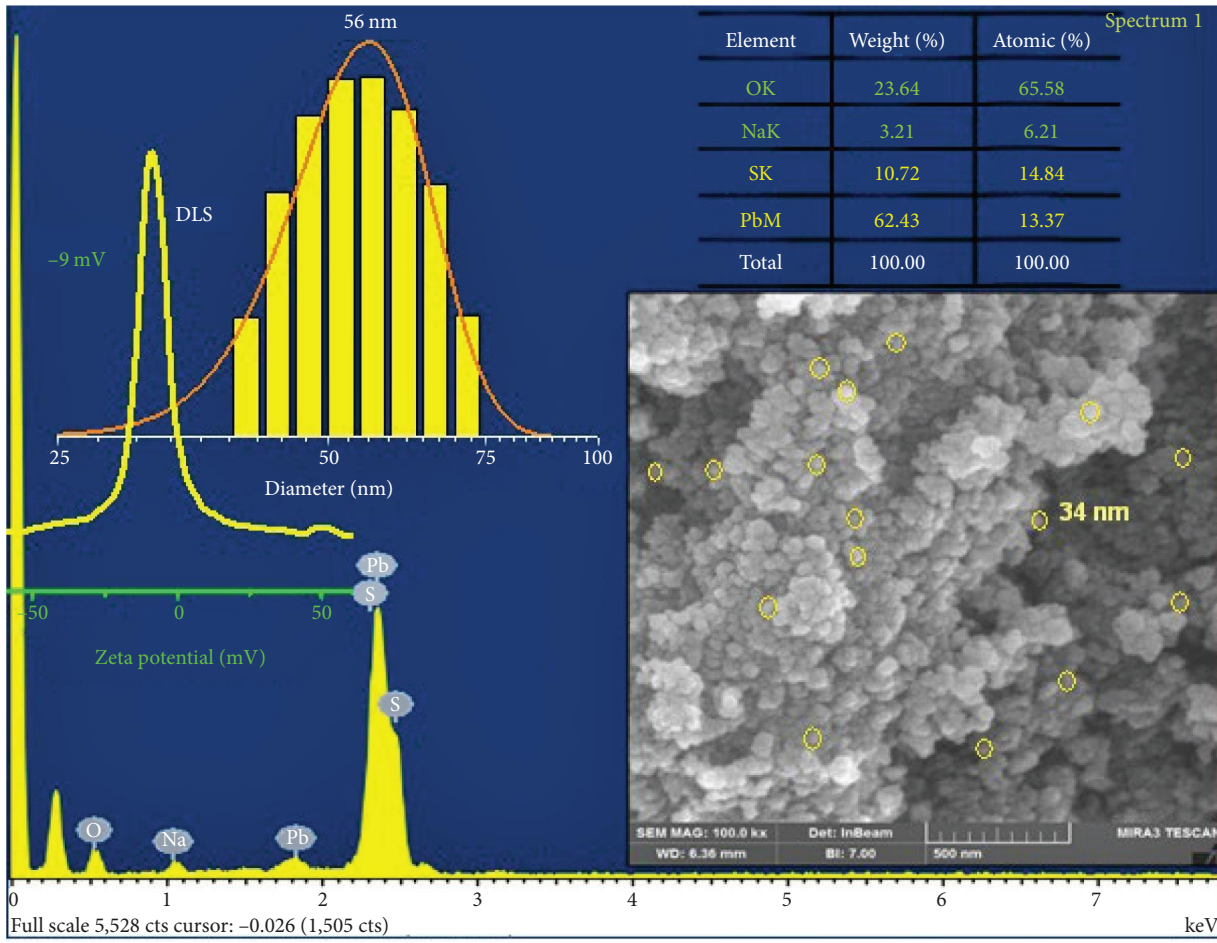

Figure 13: Number size distribution, zeta potential, EDX spectrum, and SEM picture of PbS nanopowder.

preparation of lead sulfide quantum dots with potential applications in IR detectors and solar cells.

Data Availability

The data used to support the findings of this study are available from the corresponding author upon request.

Conflicts of Interest

The author declares that there are no conflicts of interest regarding the publication of this article.

Acknowledgments

The author acknowledges the Higher Commission for Scientific Research (HCSR) in Syria for facilities and funding of this project.

References

[1] J. L. Machol, F. W. Wise, R. C. Patel, and D. B. Tanner, "Vibronic quantum beats in PbS microcrystallites," *Physical Review B*, vol. 48, no. 4, pp. 2819–2822, 1993.

[2] H. Kanazawa and S. Adachi, "Optical properties of PbS," *Journal of Applied Physics*, vol. 83, no. 11, pp. 5997–6001, 1998.

[3] L. Sun, J. J. Choi, D. Stachnik et al., "Bright infrared quantum-dot light-emitting diodes through inter-dot spacing control," *Nature Nanotechnology*, vol. 7, no. 6, pp. 369–373, 2012.

[4] C. E. Pérez-García, S. Meraz-Dávila, and F. de Moure-Flores GArreola-Jardón, "Characterization of PbS films deposited by successive ionic layer adsorption and reaction (SILAR) for CdS/PbS solar cells application," *Materials Research Express*, vol. 7, no. 1, Article ID 15530, 2020.

[5] K. W. Johnston, A. G. Pattantyus-Abraham, J. P. Clifford et al., "Schottky-quantum dot photovoltaics for efficient infrared power conversion," *Applied Physics Letters*, vol. 92, no. 15, Article ID 151115, 2008.

[6] M. Cheragizade, R. Yousefi, F. Jamali-Sheini, M. R. Mahmoudian, A. Sa´aedi, and N. Ming Huang, "Synthesis and characterization of PbS mesostructures as an IR detector grown by hydrogen-assisted thermal evaporation," *Materials Science in Semiconductor Processing*, vol. 26, pp. 704–709, 2014.

[7] E. Hechster, D. Amgar, N. Arad-Vosk et al., "Electrical and optical characterization of quantum dots PbS/TiO_2 based heterojunction as a SWIR detector and a proposed design of PbS/TiO_2-PeLED as a SWIR to visible upconversion device," *Materials Research Express*, vol. 6, no. 6, 2019.

[8] M. H. Jameel, S. Saleem, M. Hashim et al., "A comparative study on characterizations and synthesis of pure lead sulfide

(PbS) and Ag-doped PbS for photovoltaic applications," *Nanotechnology Reviews*, vol. 10, no. 1, pp. 1484–1492, 2021.

[9] E. K. Ampadu, J. Kim, E. Oh, D. Y. Lee, and K. S. Kim, "Direct chemical synthesis of PbS on large-area CVD-graphene for high-performance photovoltaic infrared photo-detectors," *Materials Letters*, vol. 277, Article ID 128323, 2020.

[10] H. Tang, J. Zhong, W. Chen et al., "Lead sulfide quantum dot photodetector with enhanced responsivity through a two-step ligand-exchange method," *ACS Applied Nano Materials*, vol. 2, no. 10, pp. 6135–6143, 2019.

[11] D. M. N. M. Dissanayake, T. Lutz, R. J. Curry, and S. R. P. Silva, "Measurement and validation of PbS nanocrystal energy levels," *Applied Physics Letters*, vol. 93, no. 4, Article ID 043501, 2008.

[12] L. F. Koao, F. G. Hone, and F. B. Dejene, "Synthesis and characterization of PbS nanowires doped with Tb^{3+}ions by using chemical bath deposition method," *Journal of Nanostructure in Chemistry*, vol. 10, no. 1, pp. 1–7, 2020.

[13] P. A. Ajibade, T. B. Mbuyazi, and A. E. Oluwalana, "Lead sulphide nanoparticles as photocatalyst for the degradation of methylene blue: effects of pH, time, adsorption kinetics and recyclability studies," *Journal of Inorganic and Organometallic Polymers and Materials*, vol. 31, no. 5, pp. 2197–2208, 2021.

[14] H. Bai, X. Li, F. Guo et al., "Comparative study on the growth mechanism of multi-shaped PbS via hydro- and solvothermal methods," *Optical Materials Express*, vol. 9, no. 2, pp. 932–943, 2019.

[15] N. H. Sheeba, A. Namitha, K. M. Ramsiya, T. M. Ashitha, and R. Suhail, "Effect of deposition time on structural and optoelectronic properties of flower-like nanostructured PbS thin films," *Journal of Scientific Research*, vol. 13, no. 1, pp. 9–20, 2021.

[16] C. Song, M. Sun, Y. Yin et al., "Synthesis of star-shaped lead sulfide (PbS) nanomaterials and theirs gas-sensing properties," *Materials Research*, vol. 19, no. 6, pp. 1351–1355, 2016.

[17] M. Salavati-Niasari, D. Ghanbari, and M. R. Loghman-Estarki, "Star-shaped PbS nanocrystals prepared by hydrothermal process in the presence of thioglycolic acid," *Polyhedron*, vol. 35, no. 1, pp. 149–153, 2012.

[18] R. Sathyamoorthy and L. Kungumadevi, "Facile synthesis of PbS nanorods induced by concentration difference," *Advanced Powder Technology*, vol. 26, no. 2, pp. 355–361, 2015.

[19] K. P. Mubiayi, N. Revaprasadu, S. S. Garje, and M. J. Moloto, "Designing the morphology of PbS nanoparticles through a single source precursor method," *Journal of Saudi Chemical Society*, vol. 21, no. 5, pp. 593–598, 2017.

[20] W. Zhu, Y. Cheng, C. Wang, N. Pinna, and X. Lu, "Transition metal sulfides meet electrospinning: versatile synthesis, distinct properties and prospective applications," *Nanoscale*, vol. 13, no. 20, pp. 9112–9146, 2021.

[21] S. Chen, L. A. Truax, and J. M. Sommers, "Alkanethiolate-protected PbS nanoclusters: synthesis, spectroscopic and electrochemical studies," *Chemistry of Materials*, vol. 12, no. 12, pp. 3864–3870, 2000.

[22] J. Ye, L. Sun, and S. Gao, "Fabrication of hollow PbS nanospheres and application in phenol release," *Springer Plus*, vol. 2, no. 1, 2013.

[23] K. Hedayati, D. Ghanbari, M. Kord, and M. Goodarzi, "(Co, Ag, Ni, Cd, Mn, Cr)-doped PbS photo-catalyst: sonochemical-assisted synthesis of magnetite nanocomposites applicable for elimination of toxic pollutants," *Journal of Materials Science: Materials in Electronics*, vol. 32, pp. 373–383, 2020.

[24] E. Yücel and Y. Yücel, "Fabrication and characterization of Sr-doped PbS thin films grown by CBD," *Ceramics International*, vol. 43, pp. 407–413, 2017.

[25] S. Rajathi, K. Kirubavathi, and K. Selvaraju, "Structural, morphological, optical, and photoluminescence properties of nanocrystalline PbS thin films grown by chemical bath deposition," *Arabian Journal of Chemistry*, vol. 10, no. 8, pp. 1167–1174, 2017.

[26] B. Abdallah, A. Ismail, H. Kashoua, and W. Zetoun, "Effects of deposition time on the morphology, structure, and optical properties of PbS thin films prepared by chemical bath deposition," *Journal of Nanomaterials*, vol. 2018, Article ID 1826959, 8 pages, 2018.

[27] K. A. Aadim, A.-M. E. Ibrahim, and J. M. Marie, "Structural and optical properties of PbS thin films deposited by pulsed laser deposited (PLD) technique at different annealing temperature," *International Journal of Physics*, vol. 5, no. 1, pp. 1–8, 2017.

[28] A. Chahadih, H. El Hamzaoui, Rémy Bernard et al., "Direct-writing of PbS nanoparticles inside transparent porous silica monoliths using pulsed femtosecond laser irradiation," *Nanoscale Research Letters*, vol. 6, no. 1, Article ID 542, 2011.

[29] Y. Zhao, X.-H. Liao, J.-M. Hong, and J.-J. Zhu, "Synthesis of lead sulfide nanocrystals via microwave and sonochemical methods," *Materials Chemistry and Physics*, vol. 87, Article ID 149, 2004.

[30] Z. R. Khan and M. Shkir, "Improved opto-nonlinear and emission properties of spray pyrolysis grown Nd: PbS nanostructured thin films," *Physica B: Condensed Matter*, vol. 627, Article ID 413612, 2022.

[31] M. F. A. Alias, A. A. J. Al-Douri, E. M. N. Al-Fawadi, and A. A. Alnajjar, "Compositional dependence of structural properties of prepared PbxS1−x alloys and films," *Advances in Condensed Matter Physics*, vol. 2011, Article ID 574979, 6 pages.

[32] S. Jemai, A. Hajjaji, F. Baig, I. Harabi, B. M. Soucase, and B. Bessais, "Crystal growth and design of various shapes of PbS micro and nanocrystals from a hydrothermal process," *Materials Characterization*, vol. 175, Article ID 111036, 2021.

[33] M. S. Dhlamini, J. J. Terblans, O. M. Ntwaeborwa, and H. C. Swart, "Synthesis and degradationof the PbS nanoparticle phosphors embedded in SiO2 (SiO2:PbS)," *Surface Review and Letters*, vol. 14, no. 4, pp. 697–701, 2007.

[34] A. S. Obaid, M. A. Mahdi, and Zainuriah Hassan, "Growth of nanocrystalline PbS thin flms by solid-vapor deposition," *Advanced Materials Research*, vol. 620, pp. 1–6, 2012.

[35] R. M. Woo-García, A. L. Herrera-May, L. García-González et al., "Structure, morphology, and local photoelectrical characterization of PbS films grown by SILAR," *Materials Letters*, vol. 314, Article ID 131844, 2022.

[36] M. Kord, K. Hedayati, and M. Farhadi, "Green synthesis and characterization of flower-like PbS and metal-doped nanostructures via hydrothermal method," *Main Group Metal Chemistry*, vol. 40, no. 1-2, pp. 35–40, 2017.

[37] E. Barrios-Salgado, Y. Rodríguez-Lazcano, J. P. Pérez-Orozco et al., "Effect of deposition time on the optoelectronics properties of PbS thin films obtained by microwave-assisted chemical bath deposition," *Advances in Condensed Matter Physics*, vol. 2019, Article ID 5960587, 8 pages, 2019.

[38] K. Paulraj, S. Ramaswamy, N. Chidhambaram, H. Algarni, M. Shkir, and S. AlFaify, "Investigation of samarium-doped PbS thin films fabricated using nebulizer spray technique for

photosensing applications," *Superlattices and Microstructures*, vol. 148, Article ID 106723, 2020.

[39] A. M. S. Arulanantham, S. Valanarasu, A. Kathalingam, and K. Jeyadheepan, "Solution volume effect on structural, optical and photovoltaic properties of nebulizer spray deposited SnS thin films," *Journal of Materials Science: Materials in Electronics*, vol. 29, no. 15, pp. 12899–12909, 2018.

[40] S. R Rosario, I. Kulandaisamy, K. D. A. Kumar, K. Ramesh, H. A. Ibrahium, and N. S. Awwad, "Ag-doped PbS thin films by nebulizer spray pyrolysis for solar cells," *International Journal of Energy Research*, vol. 1–11, 2020.

[41] S. Mlowe and N. Revaprasadu, "Preparation of spin coated PbS thin films using bis-tetrahydroquinolinedithiocarbamatolead (II) complex as a single source precursor," *Inorganic and Nano-Metal Chemistry*, vol. 52, no. 7, pp. 1019–1023, 2022.

[42] J. M. C. da Silva Filho and F. C. Marques, "Structural and optical temperature-dependent properties of PbS thin films deposited by radio frequency sputtering," *Materials Science in Semiconductor Processing*, vol. 91, pp. 188–193, 2019.

[43] F. G. Hone and F. B. Dejene, "Cationic concentration and pH effect on the structural, morphological and optical band gap of chemically synthesized lead sulfide thin films," *Journal of Materials Research and Technology*, vol. 8, no. 1, 2018.

[44] I. Alghoraibi, "Effect of deposition time on the nanocrystalline PbS thin films synthesized by chemical solution deposition method: structural characterization," *International Journal of ChemTech Research*, vol. 6, no. 5, pp. 2725–2731.

[45] H. Farshidi, A. A. Youzbashi, M. Heidari Saani, A. Rashidi, and A. Kazem Zadeh, "Control of morphology and optical properties of PbS nanostructured thin films by deposition parameters: study of mechanism," *Journal of Experimental Nanoscience*, vol. 11, no. 18, pp. 1416–1425, 2016.

[46] A. E. Madani, R. Essajai, A. Qachaou, A. Raidou, M. Fahoume, and M. Lharch, "The temperature effect on the physical properties of PbS thin films produced by the chemical bath deposition (CBD) technique," *Advances in Materials and Processing Technologies*, vol. 8, no. 3, 2021.

[47] M. Perez, M. Shandalov, Y. Golan, and T. Templeman, "Vladimir Ezersky and Eyal Yahelc, the effect of deposition mechanism on the properties of epitaxial PbS films grown from acidic bath," *Materials Chemistry Frontiers*, vol. 5, no. 6, pp. 2860–2866, 2021.

[48] A. Ganguly, S. S. Nath, and M. Choudhury, "Effect of Mn doping on multilayer PbS quantum dots sensitized solar cell," *IEEE Journal of Photovoltaics*, vol. 8, no. 6, pp. 1656–1661, 2018.

[49] H. Yıldızay, "Pinhole-Free PbS thin films obtained by chemical bath deposition method," *BSEU Journal of Science*, vol. 8, no. 2, pp. 1017–1023, 2021.

[50] F. G. Hone and F. B. Dejene, "Synthesis and characterization of lead sulphide thin films from ethanolamine (ETA) complexing agent chemical bath," *Materials Research Express*, vol. 5, no. 2, Article ID 026409, 2018.

[51] E. Yücel, "Using of CAPB as a surfactant to improve the surface morphology and optical features of PbS films," *Superlattices and Microstructures*, vol. 135, Article ID 106287, 2019.

[52] A. Ismail, M. Alahmad, H. Kashoua, M. Alsabagh, and B. Abdallah, "Structural and optical effects of low dose rate Co-60 gamma irradiation on PbS thin films," *Microelectronics Reliability*, vol. 116, Article ID 114017, 2021.

[53] A. Hussain, L. R. Singh, and S. R. Devi, "Studies on structural, optical and electrical properties of Zn-doped pbs nanocrystalline thin film," *Chalcogenide Letters*, vol. 18, no. 3, pp. 103–111, 2021.

[54] M. Liu, Q. Zhan, W. Li, R. Li, Q. He, and Y. Wang, "Effect of Zn doping concentration on optical band gap of PbS thin films," *Journal of Alloys and Compounds*, vol. 792, pp. 1000–1007, 2019.

[55] S. Rajathi, K. Kirubavathi, and K. Selvaraju, "Preparation of nanocrystalline Cd-doped PbS thin films and their structural and optical properties," *Journal of Taibah University for Science*, vol. 11, no. 6, pp. 1296–1305, 2018.

[56] K. Paulraj, S. Ramaswamy, N. Chidhambaram, H. Algarni, Mohd Shkir, and S. AlFaify, "Investigation of samarium-doped PbS thin films fabricated using nebulizer spray technique for photosensing applications," *Superlattices and Microstructures*, vol. 148, Article ID 106723, 2020.

[57] C. Rajashree and A. R. Balu, "Tuning the physical properties of PbS thin films towards optoelectronic applications through Ni doping," *Optik*, vol. 127, no. 20, pp. 8892–8898, 2016.

[58] M. Shkir, I. S. Yahia, and S. AlFaify, "A facilely one pot low temperature synthesis of novel Pt doped PbS nanopowders and their characterizations for optoelectronic applications," *Journal of Molecular Structure*, vol. 1192, pp. 68–75, 2019.

[59] M. Shkir, M. T. Khan, A. Khan, A. M. El-Toni, A. Aldalbahi, and S. AlFaify, "Facilely synthesized Cu: PbS nanoparticles and their structural, morphological, optical, dielectric and electrical studies for optoelectronic applications," *Materials Science in Semiconductor Processing*, vol. 96, pp. 16–23, 2019.

[60] K. Paulraj, S. Ramaswamy, A. M. S. Arulanantham et al., "Investigation on nebulizer spray deposited Gd-doped PbS thin flms for photo sensing applications," *Journal of Materials Science: Materials in Electronics*, vol. 30, Article ID 18858, 2019.

[61] N. F. AndradeNeto, O. B. M. Ramalho, H. Fantucci, R. M. Santos, M. R. D. Bomio, and F. V. Motta, "Fast and facile sonochemical synthesis of Mg- and Zn-doped PbS nanospheres: optical properties and photocatalytic activity," *Journal of Materials Science*, vol. 31, pp. 14192–14202, 2020.

[62] M. A. Manthrammel, S. M. Mariappan, and M. Shkir, "A facile microwave assisted synthesis of La@PbS nanoparticles and their characterizations for optoelectronics," *Journal of Inorganic and Organometallic Polymers and Materials*, vol. 32, pp. 469–477, 2022.

[63] A. M. Ahmed, M. Rabia, and M. Shaban, "The structure and photoelectrochemical activity of Cr-doped PbS thin films grown by chemical bath deposition," *RSC Advances*, vol. 10, no. 24, pp. 14458–14470, 2020.

[64] A. P. Gaiduk, P. I. Gaiduk, and A. N. Larsen, "Chemical bath deposition of PbS nanocrystals: effect of substrate," *Thin Solid Films*, vol. 516, no. 12, pp. 3791–3795, 2008.

[65] D. F. Garcia-Gutierrez, L. P. Hernandez-Casillas, M. V. Cappellari, F. Fungo, E. Martínez-Guerra, and D. I. García-Gutiérrez, "Influence of the capping ligand on the band gap and electronic levels of PbS nanoparticles through surface atomistic arrangement determination," *ACS Omega*, vol. 3, pp. 393–4035, 2018.

[66] A. popa, M. lisca, V. stancu, M. buda, E. pentia, and T. botila, "Crystallite size effect in PbS thin films grown on glass substrates by chemical bath deposition," *Journal of Optoelectronics and Advanced Materials*, vol. 8, no. 1, pp. 43–45, 2006.

[67] D. K. Sonavane, S. K. Jare, R. V. Kathare, R. N. Bulakhe, and J. J. Shim, "Chemical Synthesis of PbS Thin Films and Its physicochemical Properties," *Materials Today: Proceedings*, vol. 5, no. 2, pp. 7743–7747, 2018.

[68] B. Chatterjee and A. Bandyopadhyay, "Characterization of PbS nanoparticles synthesized using sodium lauryl sulfate at room temperature," *Materials Today: Proceedings*, vol. 76, pp. 114–119, 2023.

[69] E. Yücel and Y. Yücel, "Effect of doping concentration on the structural, morphological and optical properties of Ca-doped PbS thin films grown by CBD," *Optik*, vol. 142, pp. 82–89, 2017.

[70] S. Seghaier, N. Kamoun, R. Brini, and A. B. Amara, "Structural and optical properties of PbS thin films deposited by chemical bath deposition," *Materials Chemistry and Physics*, vol. 97, no. 1, pp. 71–80, 2006.

[71] Z. Mamiyev and N. O. Balayeva, "PbS nanostructures: a review of recent advances," *Materials Today Sustainability*, vol. 21, Article ID 100305, 2023.

[72] J. Tauc, A. Menth, and D. Wood, "Optical and magnetic investigations of the localized states in semiconducting glasses," *Physical Review Letters*, vol. 25, no. 11, Article ID 749, 1970.

[73] L. E. Brus, "Electron-electron and electron-hole interactions in small semiconductor crystallites: The size dependence of the lowest excited electronic state," *The Journal of Chemical Physics*, vol. 80, no. 9, Article ID 4403, 1984.

[74] J. R. Caram, S. N. Bertram, H. Utzat et al., "PbS nanocrystal emission is governed by multiple emissive states," *Nano Letters*, vol. 16, no. 10, Article ID 6070, 2016.

[75] J. D. Dow, "Urbach's Rule," in *Optical Properties of Highly Transparent Solids. Optical Physics and Engineering*, S. S. Mitra and B. Bendow, Eds., Springer, Boston, MA, 1975.

[76] A. H. Mohamad, S. R. Saeed, and O. G. Abdullah, "Synthesis of very-fine PbS nanoparticles dispersed homogeneously in MC matrix: effect of concentration on the structural and optical properties of host polymer," *Materials Research Express*, vol. 6, no. 11, Article ID 115332, 2019.